LAWRENCE
LIVERMORE
NATIONAL
LABORATORY

LLNL-CONF-552336

AB INITIO STUDY OF ADVANCED METALLIC NUCLEAR FUELS FOR FAST BREEDER REACTORS

A. Landa, P. Soderlind, B. Grabowski, P. E. A. Turchi, A. V. Ruban, L. Vitos

April 25, 2012

2012 MRS Spring Meeting
San Francisco, CA, United States
April 9, 2012 through April 13, 2012

Disclaimer

Ab Initio Study of Advanced Metallic Nuclear Fuels for Fast Breeder Reactors

Alexander Landa[1], Per. Söderlind[1], Blazej Grabowski[1], Patrice E.A. Turchi[1], Andrei V. Ruban[2], and Levente Vitos[2]
[1]Condensed Matter and Materials Division, Physical and Life Sciences Directorate, Lawrence Livermore National Laboratory, L-045, 7000 East Avenue, Livermore, CA 94551-0808, U.S.A.
[2]Applied Materials Physics, Department of Materials Science and Engineering, Royal Institute of Technology, Brinellvägen 23, SE-100 44 Stockholm, Sweden

ABSTRACT

Density-functional formalism is applied to study the ground state properties of γ-U-Zr and γ-U-Mo solid solutions. Calculated heats of formation are compared with CALPHAD assessments. We discuss how the heat of formation in both alloys correlates with the charge transfer between the alloy components. The decomposition curves for γ-based U-Zr and U-Mo solid solutions are derived from Ising-type Monte Carlo simulations. We explore the idea of stabilization of the δ-UZr_2 compound against the α-Zr (hcp) structure due to increase of Zr *d*-band occupancy by the addition of U to Zr. We discuss how the specific behavior of the electronic density of states in the vicinity of the Fermi level promotes the stabilization of the U_2Mo compound. The mechanism of possible Am redistribution in the U-Zr and U-Mo fuels is also discussed.

INTRODUCTION

The US Reduced Enrichment for Research and Test Reactors (RERTR) program was created in 1978 with a purpose to develop technology necessary to enable the conversion of civilian facilities using high enriched uranium (HEU, U^{235} > 85 at. %) fuels to the use of low enriched uranium (LEU, U^{235} < 20 at. %) fuels in research and test reactors [1]. In 2004 the RERTR program was absorbed into Global Treat Reduction Initiative (GTRI) [2, 3], which purpose is to reduce and protect vulnerable nuclear and radiological materials at civilian sites.

From nuclear performance standpoint, a comparable amount of fissile material (U^{235}) is required to maintain reactor power for both the LEU and HEU designs. As was mentioned in Ref. [4], the LEU design requires a fuel material with uranium density at least 5 times higher than the current HEU compounds in order to compensate for the reduction in enrichment. Another requirement for the LEU fuel is its capability to withstand the structural damage caused by the fission events occurring inside the material [4]. Early on, metallic fuels (pure U and Pu) have been considered because of their high thermal conductivity (with the very significant safety benefits) in comparison with MOX fuels (e.g., $UPuO_2$) used in thermal reactors. However, the low melting temperature of pure U, Pu, and the U-Pu alloys makes them unsuitable for high-temperature applications due to the danger of penetration of molten actinides to the cladding. That is why addition of some high-melting temperature elements, such as Cr, Mo, Nb, Re, Ru, Ti, V, or Zr, is considered in order to boost the liquidus curve in the U-Pu system thus enhancing thermal and mechanical stability [3, 5]. Alloying uranium with one of above listed high-melting temperature elements ‘stabilizes’ uranium in the bcc γ-phase in the temperature range of stability

of α-U phase. In other words, each of these high-melting temperature elements plays a role of 'γ-stabilizer' helping to keep uranium in the metastable bcc phase upon cooling.

Zirconium metal possesses a unique capability to suppress interdiffusion between the nuclear fuel and stainless-steel cladding and this makes Zr a good candidate as a solver to nuclear fuels for fast breeder reactors. The Zr-based actinide alloys, particularly U-Pu-Zr, proved to be very promising fuels for liquid metal fast breeder reactors because of their advantage in view of superior performance, reactor safety, and fuel cycle economics [6]. It was established [7] that the U-Zr system is characterized by the complete solubility of the body centered cubic high-temperature phases, γ-U and β-Zr, that is usually referred to in phase diagrams by 'γ-phase' solid solutions. Below $T \approx 722$ ^{o}C, these solutions separate into a relatively flat miscibility gap.

The intermediate δ-UZr_2 phase with C32 (AlB_2)-type structure is formed on cooling from the γ-phase with the homogeneity range from 63 to 82 at. % Zr [8]. It is well known that the high-temperature Zr-based solid solutions may transform into the so-called metastable ω-phase at low temperatures, which can also be stabilized from the α (hcp) phase of Zr under compression [9]. Ogawa *et al.* [10] suggested that the δ-UZr_2 phase could be regarded as the ω-phase solid solution that is stabilized against the α-Zr (hcp) structure by addition of U due to increase of Zr *d*-band occupancy.

Recently Kim *et al.* [11] suggested some advantages of U-TRU-Mo fuels over U-TRU-Zr in TRU-burning advanced fast nuclear reactors: U-Pu-Mo fuels have higher thermal conductivity, lower thermal expansion, and higher melting points than U-Pu-Zr fuels resulting in better safety. However, the main advantages of U-TRU-Mo fuels lies in a much lower constituent redistribution, including migration of minor actinides (MA) and lanthanides (LA) toward the cladding due to the existence of a single γ-phase over typical fuel operation temperatures. Contrary to U-Pu-Mo fuels, in U-Pu-Zr fuels MA Am redistribution is similar to that of Zr with tendency to precipitate to the center and near the fuel surface [12].

Low-enriched uranium alloys with 6 to 12 wt. % of Mo are under consideration by the GTRI program as very high density fuels (8-9 gU/cm^3 and 15-17 gU/cm^3 for dispersion-type and monolithic-type, respectively) that allow nuclear research and test reactors conversion from use of HEU to LEU fuels [4]. According to the U-Mo phase diagram [13], Mo exhibits a high solubility (~ 35 at. %) in γ-U (bcc) but below 560 ^{o}C the equilibrium state corresponds to a mixture of α-U (orthorhombic) and so-called γ`-phase, which is the U_2Mo compound with the $C11_b$ ($MoSi_2$ prototype) structure. However, by rapid cooling from the γ-phase a metastable γ-state can be retained up to room temperature.

Semi-empirical model calculations [6], supported by experimental observations, indicate that the excess enthalpy of solution of the γ-U-Zr phase controls the constituent redistribution process in the U-Zr fuels. This statement encouraged us to perform *ab initio* calculations of the heat of formation of the γ-U-Zr solid solutions [14, 15]. We later expanded our study to the ternary U-Pu-Zr system [16] as well as to the bcc alloys that plutonium forms with MA [17]. In our recent paper [18] we presented results of *ab initio* calculations of the heat of formation of the γ-U-Mo solid solutions. In this study we summarize results published in Ref. [14-18] and present results of *ab initio* calculation of the decomposition curve for the γ-U-Mo alloys. We also present results of *ab initio* calculations of the heat of formation of Am with Zr and Mo and discuss a possible mechanism of Am redistribution in the γ-U-Zr and γ-U-Mo.

THEORY

The calculations we have referred to as SR-KKRASA are performed using the scalar relativistic (SR) Green's function technique based on the KKR method within the atomic-sphere approximation (ASA) [19, 20]. For the electron exchange and correlation energy functional, the generalized gradient approximation (GGA) is adopted [21]. The equilibrium density of alloys is obtained from a Murnaghan fit [22]. In order to treat compositional disorder the KKRASA method is combined with the coherent potential approximation (CPA) [23]. The ground-state properties of the random alloys are obtained from SR-KKRASA-CPA calculations with the Coulomb screening potential and energy [24, 25]. The screening constants are determined from supercell calculations using the locally self-consistent Green's function method (LSGF) [26]. The effective cluster interactions (ECI), used in Monte Carlo (MC) simulations, are obtained from the screened generalized perturbation method (SGPM) [24, 25].

Though the KKRASA formalism is well suited to treat close-packed structures it could produce a significant error when being applied to 'open' structures, e.g., C32 or $C11_b$. That is why we also use a Green's function technique, based on the exact muffin-tin orbitals (EMTO) formalism, in present calculations, which is not limited by geometrical restrictions imposed by the ASA, and also includes the spin-obit coupling through the four-component Dirac equation [27] (relativistic effects are important for study of Pu- and Am-based systems [16, 17]). The EMTO calculations are performed using both scalar-relativistic and fully-relativistic (FR) Green's function techniques based on the improved screened KKR method [28]. The total energy is obtained from the full charge-density technique [29] and GGA is used for the electron exchange and correlation approximation. EMTO is combined with the CPA for calculation of the total energy of chemically random alloy [30]. The choice of the screening constants is identical to those in the SR-KKRASA method. Although spin-polarization is not considered in the case of the U-Zr and U-Mo systems, the Pu- and Am-based alloys are modeled within the disordered local moment (DLM) approximation that leads to a paramagnetic solution (see Ref. [31]).

For the elemental metals, the most accurate and fully-relativistic calculations are performed using an all-electron approach where the relativistic effects, including spin-orbit coupling, are accounted for. Although unable to model disorder in the CPA sense it provides important information for the metals, and also serves to confirm the CPA calculations mentioned above. For this purpose we use a version of the FPLMTO [32]. As in the case of the KKRASA and EMTO methods, GGA is used for the electron exchange-correlation approximation. A special quasi-random structure (SQS) method is used to treat the compositional disorder within the FPLMTO formalism [33]. Spin polarization for the Pu-containing alloys is arranged in an antiferromagnetic fashion [34] with neighboring atoms having anti-parallel spins. This is different from the spin configuration used in the EMTO calculations that assumes spin disorder.

Due to significant size mismatch between U and Mo atoms, it is necessary to account 'stain-induced' contribution to ECI in addition to 'chemical' contribution obtained from SGPM. This 'elastic' contribution to ECI is derived from the structure inverse Connelly-Williams (CW) method [35] on the basis of the total relaxation energies of 29 ordered structure equally distributed around the equiatomic composition. The calculations of the relaxations energies are performed within the projector augmented wave (PAW) method as implemented in the VASP software package [36, 37] in combination with the provided PAW potentials [38]. GGA is used for the electron exchange-correlation approximation.

DISCUSSION

U-Zr system

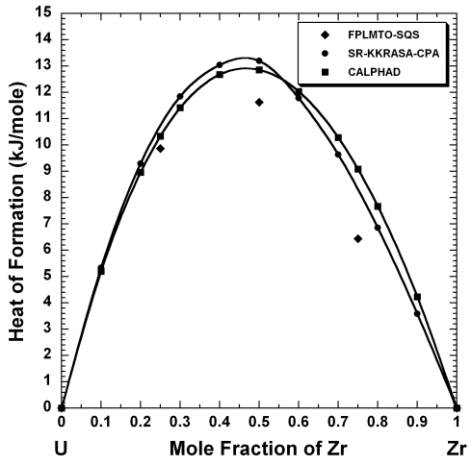

Figure 1. The heat of formation versus composition calculated at $T = 0$ K for the γ-U-Zr alloys.

Figure 1 shows the results of SR-KKRASA-CPA calculations of the heat of formation of the γ-U-Zr solid solutions at $T = 0$ K. The heat of formation shows a positive deviation from the Vegard's law that agrees well with the existence of a miscibility gap in the U-Zr phase diagram. Notice that the calculated heat of formation of the γ-U-Zr solid solutions is in excellent agreement with data extracted from the experimental phase diagram by the use of CALPHAD methodology [39], which suggests a robustness of the *ab initio* approach. For comparison, we also show the heats of formation for the $U_{75}Zr_{25}$, $U_{50}Zr_{50}$, and $U_{25}Zr_{75}$ bcc alloys calculated within the FPLMTO-SQS technique that agree pretty well with both SR-KKRASA-CPA and CALPHAD assessment results.

We performed Ising-type MC calculations of the decomposition curve for the γ-U-Zr solid solutions. The MC simulations are performed using the Metropolis algorithm [40] for a 1728-site simulation box (12 • 12 • 12) with periodic boundary conditions. Figure 2 displays the calculated temperature of decomposition of the γ-$U_{1-c}Zr_c$ alloys within the wide range of composition. This curve has a maximum that is located somewhere between 20 and 30 at. % of zirconium. This maximum matches relatively well the location of the maximum on the experimental miscibility gap (~ 30 at. % of zirconium) also shown in the figure.

It is well established that under compression zirconium metal undergoes the following phase transformations: α-Zr (hcp) $\rightarrow$ ω-Zr (C32) $\rightarrow$ β-Zr (bcc) [9, 42]. According to the FPLMTO calculations, the $\alpha \rightarrow \omega$ and $\omega \rightarrow \beta$ phase transitions in Zr take place at 33 and 268 kbar, respectively, which are in a good accord with experimental measurements [9, 42]. Figure 3 (a) shows results of FPLMTO calculations of the *s*-, *p*-, and *d*-band occupations change in α-Zr as a function of the Wigner-Seitz radius (pressure). As pressure increases, the occupation of the *d*-band goes up due to a loss of the *s*- and *p*-band electrons. In Figure 3 (b) we show the structural-energy difference obtained from canonical bands [43] as a function of *d*-band filling. One can see that as the *d*-band occupation increases under compression, hcp transforms to C32 and then to bcc.

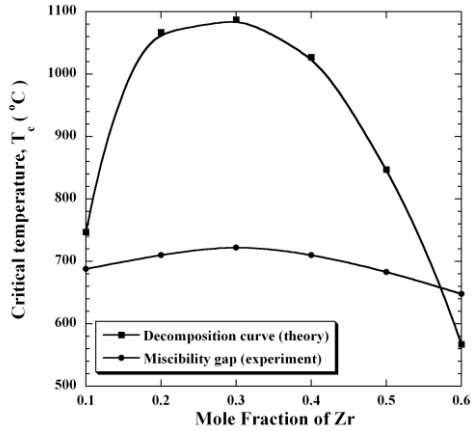

Figure 2. Temperature of decomposition of the γ-U-Zr alloys. Experimental data on the miscibility gap are taken from Ref. [41].

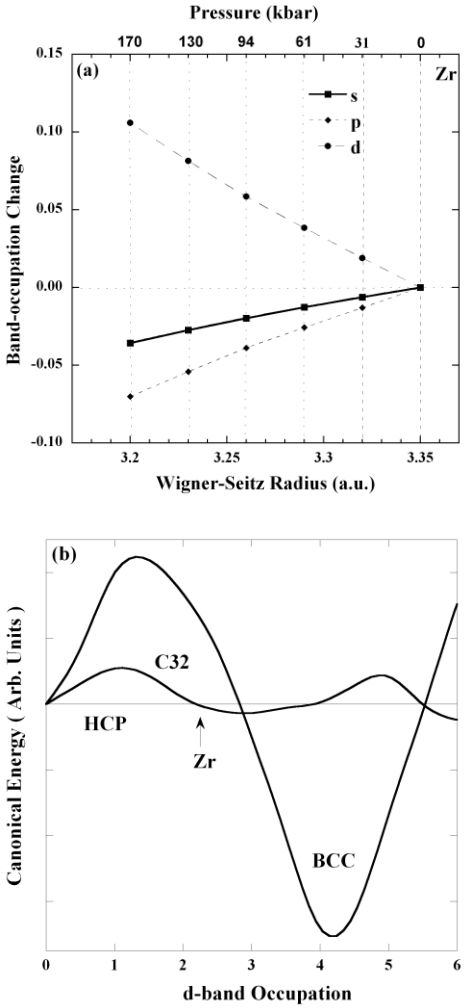

Figure 3. The change in band occupations in α-Zr under compression (a); the energy difference obtained from canonical *d*-bands calculations as a function of *d*-band occupancy (b). The hcp phase is used as the reference point and is set equal to zero.

Next, we discuss the analogies with the U-Zr system. Figure 4 has two parts. The upper part shows how the *d*-band occupation of α-Zr changes under compression and the transition region (full black) spans betweens the lower and upper experimental bounds, 21 kbar and 85 kbar [9, 42], of the $\alpha \rightarrow \omega$ transformation. The hatched patch of the upper part of the plot shows the pressure region of the certain ω-phase stability in pure Zr. The lower part of this plot shows how the *d*-band occupation changes as a function of an increase in U composition in the U-Zr system. The hatched part of this part of the plot spans within the range of the homogeneity of the δ-U-Zr phase (18 – 37 at. % of uranium [8]). One can see that at the upper pressure border of the $\alpha \rightarrow \omega$ phase transition range in pure Zr (~ 85 kbar) its *d*-occupation almost reaches the same value as it has when composition of uranium, alloyed with α-Zr, reaches the value ~ 18 at. %, [8] when the δ-UZr_2 phase starts to form. Thus the present calculations confirm the hypothesis [10] that stabilization of the δ-UZr_2 phase has the same origin as that of the ω-phase in pure Zr under compression, namely, it is induced by an increase in *d*-band filling.

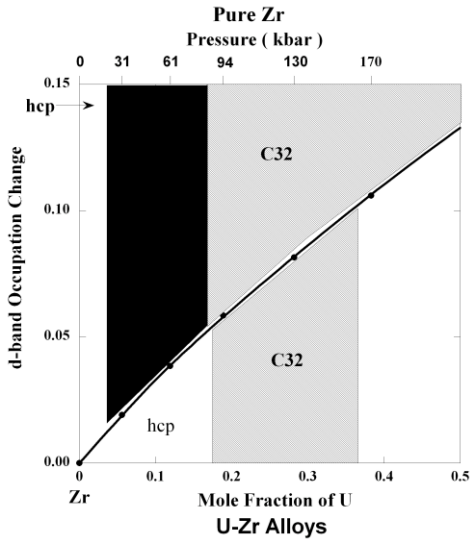

Figure 4. Comparison of *d*-band occupancy in α-Zr as a function of compression with *d*-band occupancy in the U-Zr hcp alloys as a function of U concentration.

U-Mo system

Figure 5 show results of SR-EMTO-CPA calculations of the heat of formation of the γ-U-Mo solid solutions at T = 0 K. The calculated heat of formation is positive in a broad region of the composition interval of the U-Mo phase diagram but changes it sign from positive to negative when uranium composition exceeds ~ 80 at. %. For comparison, we also show the heats of formation for the $U_{75}Mo_{25}$, $U_{50}Mo_{50}$, and $U_{25}Mo_{75}$ bcc alloys, calculated within the SR-FPLMTO- SQS technique that agrees pretty well with SR-EMTO-CPA results. A good agreement between the results derived by different methods, e.g., SR-EMTO-CPA and SR-FPLMTO- SQS results for the $U_{50}Mo_{50}$ alloy are almost identical, suggests a robustness of the both *ab initio* approaches applied to study the γ-U-Mo solid solutions. This plot also shows CAPHAD assessment [44] of the heat of formation of the γ-U-Mo solid solutions at T = 100 K with a distinctive change of its sign from positive to negative around 80 at. % of uranium.

Within the EMTO formalism [28], the total-energy, E_{tot}, can be expressed as the sum of

two contributions: $E_{tot} = E_b + E_M$, where E_b consists of all "local" (band-structure) contributions, $E_b = E_s + E_{intra} + E_{xc}$, such as the kinetic energy of non-interacting electron gas, E_s, the intra-cell electrostatic energy, E_{intra}, which is due to the electron-electron and electron-ion Coulomb interactions, and the exchange and correlation energy, E_{xc}. The remaining contribution, E_M, is the inter-cell Madelung energy. A similar decomposition of the total energy is possible within the KKRASA formalism.

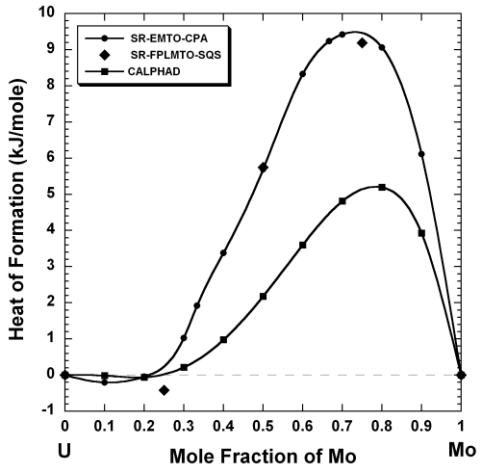

Figure 5. The heat of formation versus composition calculated at $T = 0$ K for the γ-U-Mo alloys.

Table I. Equilibrium Wigner-Seitz radius, S_{WS}, (in a.u.), screening constants, α and β, charge transfer from U atoms, ΔQ_U, contributions, ΔE_b and ΔE_M, to the heat of formation, ΔE_{tot}, (in kJ/mole) of the bcc $U_{50}Mo_{50}$ and $U_{50}Zr_{50}$ alloys.

Alloy	S_{WS}	α	β	ΔQ_U	ΔE_b	ΔE_M	ΔE_{tot}
$U_{50}Mo_{50}$	3.1274	0.725	1.088	-0.440	74.5648	-68.8681	5.6967
$U_{50}Zr_{50}$	3.3163	0.700	1.060	-0.248	32.4705	-19.5332	12.9373

In the Table 1 we compare the results of our calculated heat of formation, ΔE_{tot}, of bcc $U_{50}Mo_{50}$ and $U_{50}Zr_{50}$ alloys. This Table also lists the energy contributions, ΔE_b, and ΔE_M, the equilibrium Wigner-Seitz radius, S_{WS}, the screening constants, α and β, and the charge transfer from uranium atoms, ΔQ_U. According to Ref. [25], the Madelung energy contribution to the heat of formation of a disordered A_cB_{1-c} alloy is proportional to $\left(-\alpha \frac{(\Delta Q)^2}{S_{ws}} \beta c(1-c)\right)$, where c is the concentration of the component 'A'. The Madelung energy contribution to the heat of formation of a disordered alloy is always negative and, as one can see from the Table 1, the absolute value of this contribution for the $U_{50}Mo_{50}$ alloy is ~3.53 larger than for the $U_{50}Zr_{50}$ alloy. This ponderable negative Madelung energy contribution to the heat of formation of the $U_{50}Mo_{50}$ alloy in comparison with one for the $U_{50}Zr_{50}$ alloy is predominantly due to a significantly larger absolute value of the charge transfer from uranium atoms in the case of the U-Mo alloys than in the case of the U-Zr alloys. Even the band-structure contribution to the heat of formation, ΔE_b, is positive and ~2.30 larger for the $U_{50}Mo_{50}$ alloy than for the $U_{50}Zr_{50}$ alloy, the large negative Madelung energy contribution prevails in the case of the $U_{50}Mo_{50}$ alloy resulting in a drop of the

heat of formation of this alloy by the factor of ~2.27 in comparison with the $U_{50}Zr_{50}$ alloy.

In order to explain why the disordered γ-U_2Mo alloy is unstable with respect to the ordering to the U_2Mo ($C11_b$) structure, we plot the total electronic density of states (DOS) for this disordered and ordered U_2Mo alloy (Figure 6). One can see that there is a significant drop of the DOS in the vicinity of the Fermi level (E_F) in the case of the ordered ($C11_b$) compound that causes a decrease of the band-structure contribution (E_b) to the total energy.

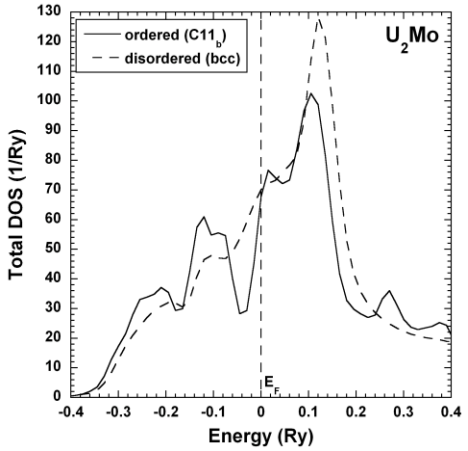

Figure 6. The DOS versus energy calculated for the U-Mo system (the Fermi energy is selected as zero energy).

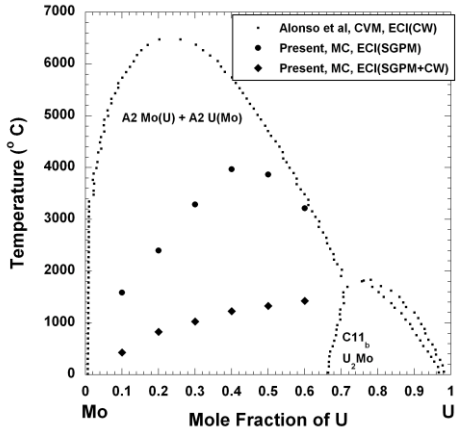

Figure 7. Calculated bcc phase diagram of the U-Mo system by Alonso *et. al.* [45]. Results of present MC calculations of temperature of decomposition of the γ-U-Mo alloys are also shown.

So far there has only been one attempt [45] to perform *ab initio* study of the formation energy of γ-U-Mo solid solutions. Using the cluster expansion technique within the Ising Hamiltonian formalism with a set of ECI defined by the CW method, these authors calculated the formation energy of the disordered γ-U-Mo solid solutions. However, temperatures of calculated by the cluster variational method (CVM) phase equilibria were excessively high [45]. Results of these calculations are presented on Figure 7 together with results of present MC calculations of temperature of decomposition of the γ-U-Mo alloys. The setup for our calculations for the γ-U-Mo alloys is identical to one performed for the γ-U-Zr alloys, described above, except that we not only performed MC calculations with ECI obtained from SGPM (shown as MC,

ECI(SGPM)) but also performed MC calculations with ECI corrected by the 'strain-induced' contribution derived from the CW method (shown as MC, ECI(SGPM+CW)). Ability to account compositional dependence of ECI within the SGPM formalism significantly decreases temperature of decomposition of the γ-U-Mo solid solutions in comparison with data obtained by Alonso *et. al.* [45] and further account for elastic contribution to ECI produces even lower temperature of decomposition of the γ-U-Mo solid solutions.

U-Zr-Am and U-Mo-Am systems

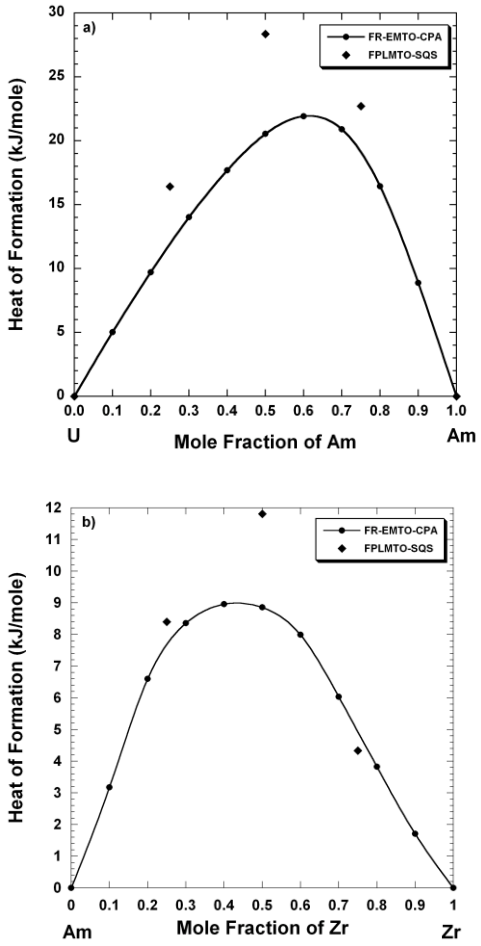

Figure 8. The heat of formation versus composition calculated at T = 0 K for a) γ-U-Am and b) γ-Am-Zr alloys.

Figure 8 show results of FR-EMTO-CPA calculations of the heat of formation of γ-U-Am and γ-Am-Zr solid solutions at T = 0 K. The heat of formation for the γ-U-Am (γ-Am-Zr) solid solutions is positive and larger (smaller) that one of the γ-U-Zr solid solutions (see Figure 1). That means that in some temperature range bellow the highest 'phase separation temperature' for γ-U-Zr alloys (see Figure 2), Am can form solid solutions with Zr but not with U. These results are in accord with observation of Kim *et. al.* [12] who found that Am redistribution in Pu-U-Zr fuels is similar to that of Zr with tendency to precipitate to the center and near the fuel surface.

For comparison, we also show the heats of formation for $Am_{75}U(Zr)_{25}$, $Am_{50}U(Zr)_{50}$, and $Am_{25}U(Zr)_{75}$ bcc alloys, calculated within the FPLMTO-SQS technique, The FPLMTO-SQS results for the $Am_{75}U(Zr)_{25}$ and $Am_{25}U(Zr)_{75}$ bcc alloys agree relatively well with FR-EMTO-CPA results but the FPLMTO-SQS model for the $Am_{50}U(Zr)_{50}$ alloys show larger heat of formations. The same trend was previously reported also for the γ-$Pu_{50}U_{50}$ alloy (see Figure 1b from Ref. [16]). We speculate that the SQS supercell for the 50% concentration, which is different than that for the 25% and 75%, may not be as well representing the true disordered alloy. Perhaps a larger supercell could remedy this but that would imply significantly more computational effort.

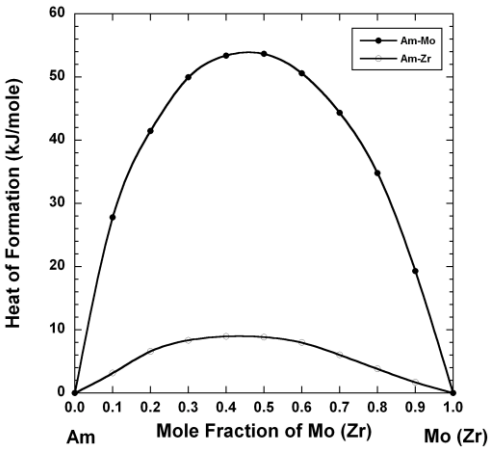

Figure 9. The heat of formation versus composition calculated at $T = 0$ K for γ-Am-Mo and γ-Am-Zr alloys.

In Figure 9 we compare the results of FR-EMTO-CPA calculations of the heat of formation of the γ-Am-Mo and γ-Am-Zr alloys. By comparing the heats of formation for these alloys one can see that, within the range of typical nuclear fuel operation temperatures, γ-Am can form solid solutions with β-Zr but not with α-Mo. The obvious reason of γ-Am and α-Mo immiscibility is a significant size mismatch of these metals.

CONCLUSIONS

In the present paper *ab initio* results are obtained for U-Zr and U-Mo alloys to understand the effectiveness of the first-principle methods in describing actinide alloys that could be used as fuels for TRU-burning fast reactors. Ability of Zr and Mo to play a role of 'γ-stabilizers' helping to keep U in the metastable bcc phase upon cooling is discussed. Our calculations suggest the physical origin of a very week constituent redistribution in γ-U-Mo fuels in comparison with their γ-U-Zr counterparts is connected to significant larger charge transfer in the U-Mo alloys than in the U-Zr alloys. Results of MC calculations of temperature of decomposition of the γ-U-Zr and γ-U-Mo alloys are presented. Stabilization of the C32-phase in the U-Zr system is explained in terms of *d*-band occupation increase as U is alloyed with Zr. Stabilization of the $C11_b$-phase in the U-Mo system is explained in terms of the electronic DOS change due to

ordering of the U_2Mo alloy. The possible mechanism of Am redistribution in the U-Zr and U-Mo fuels is discussed. These *ab initio* results will be used to build a thermodynamic database with important input from first-principles theory that will be directly comparable to the results obtained solely from experimental data on thermodynamic properties and phase diagrams. With an improved and validated coupling between *ab initio* and CALPHAD, the thermodynamic driving force associated with any actinide-based alloy will be used as input for predicting microstructure evolution and site redistribution.

ACKNOWLEDGMENTS

This work was performed under the auspices of the US Department of Energy by Lawrence Livermore National Laboratory under Contract DE-AC52-07NA27344. Work at LLNL was funded by the Laboratory Directed Research and Development Program at LLNL under project tracking code 12-SI-008. Financial support from the DOE-NE NEAMS Program is gratefully acknowledged.

REFERENCES

1. J. L. Snelgrove, G. L. Hofman, M. K. Mayer, C. L. Trybus, and T. C. Wiencek, *Nucl. Eng. Des.* **178**, 119 (1997).
2. P. Staples, in: *Transactions of 14th Inernational Topical Meeting on Research Reactor Fuel Management (RRFM 2010)*, (ENS-IAEA, Marrakech, Morocco (2010) Session 1, pp. 1-6.
3. S. Neogy, M. T. Saify, S. K. Jha, D. Srivastava, M. M. Hussain, G. K. Dey, and R. P. Singh, *J. Nucl. Mater.* **422**, 77 (2012).
4. D. M. Wachs, Nuclear Engineering International, 08 March 2010, pp. 1-6.
5. V. P. Sinha, P. V. Hegde, G. J. Prasad, G. K. Dey, and H. S. Kamath, *J. Alloys Compd.* **491**, 753 (2010).
6. G. L. Hofman, L. C. Walters, and T. H. Bauer, *Progr. Nucl. Energy* (1/2) 83 (1997).
7. M. Akabori, A. Itoh, T. Ogawa, F. Kobayashi, and Y. Suzuki, *J. Nucl. Mater.* **188**, 249 (1992).
8. T. Ogawa, M. Akabori, A. Itoh, and T. Ogawa, *J. Nucl. Mater.* **232**, 125 (1996).
9. S. K. Sikka, Y. K. Vohra, and R. Chidambaran, *Prog. Mater. Sci.* **27**, 245 (1982).
10. T. Ogawa, J. K. Gibson, R. G. Haire, M. M. Gensini, and M. Akabori, *J. Nucl. Mater.* **223**, 67 (1995).
11. Y. -S. Kim, G. L. Hofman, A. M. Yacout, and T. -K. Kim, in: *Proceedings of International Conference on Fast Reactors and Related Fuel Cycles (FR09), Challenges and Opportunities*, edited by T. Okazaki, J. Bouchard, T. Takeda, and Y. Oka (I A E A-CN-176, Kyoto, Japan, 2009) pp. 1-9.
12. Y. -S. Kim, G. L. Hofman, S. L. Hayes, and Y. -H. Sohn, *J. Nucl. Mater.* **327**, 27 (2004).
13. H. Okamoto, in: *Binary Alloys Phase Diagrams, 2nd Ed.*, edited by T. B. Massalski, (ASM International, Materials Park, Ohio 1990) Vol. 3 p. 2682.
14. A. Landa, P. Söderlind, and P. E. A. Turchi, *J. Alloys Comp.* **478**, 103 (2009).
15. A. Landa, P. Söderlind, P. E. A. Turchi, L. Vitos, and A. Ruban, J. *Nucl. Mater.* **385**, 68

(2009).
16. A. Landa, P. Söderlind, P. E. A. Turchi, L. Vitos, and A. Ruban, *J. Nucl. Mater.* **393**, 141 (2009).
17. A. Landa, P. Söderlind, P. E. A. Turchi, L. Vitos, O. E. Peil, and A.V. Ruban, *J. Nucl. Mater.* **408**, 61 (2011).
18. A. Landa, P. Söderlind, and P. E. A. Turchi, *J. Nucl. Mater*. **414**, 132 (2011).
19. I. A. Abrikosov and H. L. Skriver, *Phys. Rev.* **B47**, 16532 (1993).
20. A. V. Ruban and H. L. Skriver, *Comput. Mater. Sci.* **15**, 119 (1999).
21. J. P. Perdew, K. Burke, and M. Ernzerhof, *Phys. Rev. Lett*. **77**, 3865 (1996).
22. F. D. Murnaghan, *Proc. Natl. Acad. Sci. U.S.A.* **30**, 244 (1944).
23. J. S. Faulkner, *Prog. Mater. Sci.* **27**, 1 (1982).
24. A. V. Ruban and H. L. Skriver, *Phys. Rev.* **B66**, 024201 (2002).
25. A. V. Ruban, S. I. Simak, P. A. Korzhavyi, and H. L. Skriver, *Phys. Rev.* **B66**, 024202 (2002).
26. I. A. Abrikosov, S. I. Simak, B. Johansson, A. V. Ruban, and H. L. Skriver, *Phys. Rev.* **B56**, 9319 (1997).
27. L. V. Pourovskii, A. V. Ruban, L. Vitos, H. Ebert, B. Johansson, and I. A. Abrikosov, *Phys. Rev.* **B71**, 094415 (2005).
28. L. Vitos, *Computational Quantum Mechanics for Materials Engineers: The EMTO Method and Applications* (Springer-Verlag, London, 2007).
29. J. Kollar, L. Vitos, and H. L. Skriver, in: *Electronic Structure and Physical Properties of Solids: The Uses of the LMTO Method, Lecture Notes in Physics*, edited by H. Dreyssé (Springer-Verlag, Berlin, 2000) pp. 85-113.
30. L. Vitos, I. A. Abrikosov, and B. Johansson, *Phys. Rev. Lett.* **87**, 156401 (2001).
31. P. Söderlind, A. Landa, and B. Sadigh, *Phys. Rev.* **B66**, 205109 (2002).
32. J. M. Wills, O. Eriksson, M. Alouani, and D. L. Price, in: *Electronic Structure and Physical Properties of Solids: The Uses of the LMTO Method*, edited by H. Dreyssé (Springer-Verlag, Berlin, 2000), pp.148-167.
33. A. Zunger, S. H. Wei, L. G. Ferreira, and J. E. Bernard, *Phys. Rev. Lett.* **65**, 353 (1990).
34. P. Söderlind, Europhys. Lett. **55**, 525 (2001); P. Söderlind and B. Sadigh, Phys. Rev. Lett **92**, 185702 (2004).
35. J. W. D. Connoly and A. R. Williams, *Phys. Rev.* **B27**, 5169 (1983).
36. G. Kresse and J. Furthmüller, *Phys. Rev*. **B54**, 11169 (1996).
37. G. Kresse and J. Furthmüller, *Comput. Mater. Sci*. **6**, 15 (1996).
38. G. Kresse and D. Joubert, *Phys. Rev.* **B59**, 1758 (1999).
39. P. E. A. Turchi, I. A. Abrikosov, B. Burton, S. G. Fries, G. Grimvall, L. Kauffman, P. Korzhavyi, V. Rao Manga, M. Ohno, A. Pisch, A. Scott, and W. Zhang, *CALPHAD* **31**, 4 (2007).
40. K. Binder, *Application of the Monte Carlo Method in Statistical Physics* (Springer-Verlag, Berlin, 1987)
41. H. Okamoto, *J. Phase Equilib*. **14** (2), 267 (1993).
42. C. W. Greeff, *Modeling Simul. Mater. Sci. Eng.* **13**, 1015 (2005).
43. H. L. Skriver, *Phys. Rev.* **B31**, 1909 (1985).
44. X. Zhang, Y. F. Cui, G. L. Xu, W.J. Zhu, H. S. Liu, B. Y. Yin, and Z.P. Jin, *J. Nucl. Mater.* **402**, 15 (2010).
45. P. R. Alonso and G. H. Rubiolo, *Modeling. Simul. Mater. Sci. Eng*. **15**, 263 (2007).